Generated Pattern Current for Electro-Dissolution: Surface Leveling Enhancement, Diffusion Layer Control, and Thermal Stabilization in Electropolishing and Electrochemical Machining

Ibrahim Karakoc

GigaPulse Energy, Izmir, Turkey | ibrahim@gigapulse.energy

PCT/TR2025/051176 | USPTO Appl. No. 19/298,223 | Priority Date: July 23, 2025

Abstract

Electro-dissolution — the controlled anodic removal of metal into ionic species — underpins electropolishing, electrochemical machining (ECM), and electrochemical microfabrication. Three concurrent physical phenomena determine dissolution quality: local current distribution at surface micro-topography features that governs surface leveling selectivity, diffusion layer accumulation of dissolved metal ions that produces concentration polarization and limits dissolution rate, and Joule heating that introduces thermal gradients causing geometric distortion in precision ECM applications. Conventional constant current (CC) electro-dissolution applies a temporally invariant anodic current that cannot independently address these three phenomena.

This paper presents the application of the Generated Pattern Current (GPC) paradigm, implemented through the Dynamic Defined Pattern Charging (DDPC) framework, to electro-dissolution. GPC is the electrochemical symmetry counterpart of GPC electroplating (Paper 9 [26] of this series [26]): the same diffusion layer physics and Butler-Volmer nonlinearity apply, but with anodic rather than cathodic current direction. GPC applies a three-phase temporal anodic current: an aggressive dissolution phase that exploits the nonlinear Butler-Volmer selectivity between surface micro-peaks and valleys; a controlled removal phase at moderate anodic current; and an ion-clearing relaxation phase during which dissolved metal ions diffuse away from the surface, restoring the diffusion boundary layer. Faraday's law of electrolysis guarantees that the total dissolved mass [Eq. (3)] depends only on the time-averaged current, so GPC preserves the material removal rate (MRR) while improving surface quality and geometric accuracy. Theoretical predictions include 30–50% reduction in surface roughness Ra, suppression of micro-pitting, improved geometric accuracy in ECM, and extended bath life through reduced diffusion layer saturation.

The novelty of GPC electro-dissolution lies in treating temporal current structure as an independent engineering variable in anodic dissolution processes. Existing electropolishing and ECM literature has optimized electrolyte chemistry, electrode geometry, flow conditions, and workpiece material — but has not systematically exploited the temporal dimension of the applied current as a control handle for simultaneously addressing surface leveling, diffusion layer dynamics, and thermal management. GPC fills this gap by providing a rigorous theoretical foundation based on Jensen's inequality and Faraday's law invariance, and a practical three-phase protocol architecture that is deployable on existing industrial electro-dissolution equipment without hardware modification [1,2].

Keywords: Generated Pattern Current (GPC); electro-dissolution; electropolishing; electrochemical machining (ECM); surface leveling

1. Introduction

1.1 Electro-Dissolution and Industrial Applications

Electro-dissolution encompasses all processes in which a metal anode is dissolved into solution by an externally imposed anodic current. The dissolution reaction follows Eq. (1):

$$M \rightarrow M^{(z+)} + ze^{-} \quad (1)$$

where M is the metal being dissolved, z is the number of electrons transferred per metal ion (valence), and e^{-} denotes an electron.

Four major industrial application domains exploit this reaction. Electropolishing applies anodic dissolution in concentrated acid electrolytes to reduce surface roughness on stainless steel medical devices, food processing equipment, semiconductor wafer holders, and precision optical components [2,3,7]. The leveling mechanism relies on preferential dissolution at surface micro-peaks, where the local current density j is higher due to the thinner diffusion layer and more intense electric field. Electrochemical machining (ECM) applies high current density (5–200 A/cm²) with continuously refreshed electrolyte to machine hard metals—nickel superalloys, titanium, hardened steel—to complex geometries that are difficult or impossible to achieve by conventional cutting [4,5,6]. Electrochemical microfabrication applies the same principles at the microscale to produce MEMS components, micro-channels, and high-aspect-ratio features in biomedical and aerospace applications [3,7]. Corrosion testing uses controlled anodic dissolution to characterize metal corrosion resistance by measuring dissolution current as a function of potential [9].

Across all four application domains, the quality of the dissolution outcome—surface roughness Ra, pit density, geometric accuracy of machined features, dissolution current uniformity—depends on the temporal structure of the applied anodic current. Conventional CC electro-dissolution applies an invariant anodic current that simultaneously drives all three quality-limiting phenomena, preventing independent optimization.

1.2 Three Quality-Limiting Phenomena

Surface leveling selectivity is the primary quality metric of electropolishing. The leveling mechanism relies on the difference in local current density between micro-peaks (higher j, thinner local diffusion layer) and micro-valleys (lower j, thicker local diffusion layer) [2,7]. This selectivity peaks when the viscous diffusion layer thickness δ is comparable to the surface roughness amplitude R_a—the Jacquet condition. Under CC electropolishing, the diffusion layer thickens progressively as dissolved metal ions accumulate near the surface, reducing the peak-to-valley j contrast and degrading leveling selectivity over time. Additionally, the high local current density at micro-peaks can produce micro-pitting through localized transpassive dissolution if the potential exceeds the transpassive threshold [2,3].

Diffusion layer accumulation of dissolved M^(z+) ions creates concentration polarization that opposes further dissolution. The diffusion layer of thickness δ grows under CC operation as shown in Eq. (2):

$$C_s(t) = C_s,0 + j \cdot t / (z \cdot F \cdot D/\delta) \quad (2)$$

where C_s is the surface concentration of dissolved ions, D is the diffusion coefficient of M^(z+), and C_s,0 is the bulk concentration. As C_s approaches the saturation concentration C_sat, the dissolution rate is limited by mass transport rather than charge transfer kinetics, and the current efficiency drops [7,8]. In ECM with flowing electrolyte, forced convection limits diffusion layer growth but cannot eliminate it entirely at high current densities.

Joule heating in ECM generates thermal gradients that cause workpiece thermal expansion during machining. The power dissipated per unit area P = j·V_cell produces temperature increases ΔT = P·R_thermal in the inter-electrode gap. For precision ECM of aerospace turbine blade cooling channels, thermal deformation of 1–5 μm is significant relative to the required dimensional tolerance. Under CC, the continuous power dissipation maintains a steady-state thermal distortion that must be compensated by dimensional allowances in the tool design [4,5].

1.3 Limitations of CC and Pulse Reverse Electro-Dissolution

CC electro-dissolution cannot independently control leveling selectivity, diffusion layer thickness, and Joule heating because all three are monotonic functions of the applied current density. Increasing j improves dissolution rate but worsens diffusion layer accumulation and Joule heating; decreasing j reduces thermal gradients but also reduces leveling selectivity and MRR.

Pulse reverse (PR) electro-dissolution—alternating cathodic pulses with the anodic dissolution current—has been explored for electropolishing [3,12,13]. The cathodic phase partially replates dissolved ions onto the surface, preferentially at concave sites (valleys), which can improve leveling. However, the cathodic redeposition consumes charge without contributing to net dissolution, reducing current efficiency relative to CC. The fixed pulse parameters (anodic:cathodic time ratio and amplitude) cannot adapt to the evolving surface state. GPC eliminates the cathodic redeposition penalty by using low-current anodic phases for ion clearing rather than cathodic reversal.

1.4 GPC as Temporal Anodic Current Design

Generated Pattern Current (GPC), protected under PCT/TR2025/051176 and USPTO Application No. 19/298,223 (priority date July 23, 2025), applies temporally structured anodic current I(t) to the dissolution cell. The theoretical foundation is identical to GPC electroplating (Paper 9 [26] [26]): Jensen's inequality applied to the nonlinear Butler-Volmer kinetics:

$$f(\bar{I}) \neq \langle f(I(t)) \rangle$$

where f represents any nonlinear dissolution response. Faraday's law guarantees that the total dissolved mass m = ⟨I⟩·t·M/(z·F) depends only on the time-averaged anodic current ⟨I⟩, so GPC preserves the MRR identically to CC at the same ⟨I⟩ while changing the temporal distribution to improve surface quality and geometric accuracy. This is the electrochemical

symmetry argument: the same physics that GPC exploits in cathodic deposition (Paper 9 [26] [26]) applies in reversed polarity to anodic dissolution.

1.5 Scope

Section 2 presents the electro-dissolution electrochemical physics. Section 3 analyzes the three GPC quality mechanisms. Section 4 describes GPC protocol design including GigaPulse Lab implementation. Section 5 addresses electropolishing, ECM, and microfabrication application-specific considerations. Section 6 quantifies expected outcomes. Section 7 presents the experimental validation framework. Section 8 discusses the electrochemical symmetry with GPC electroplating. Section 9 concludes.

2. Electro-Dissolution Electrochemical Physics

2.1 Faraday's Law and MRR Invariance

The total dissolved mass is governed by Faraday's law:

$$m = \langle I \rangle \cdot t \cdot M / (z \cdot F) \quad (3)$$

The material removal rate (MRR) is given by Eq. (4):

$$MRR = \langle I \rangle \cdot M / (z \cdot F \cdot \rho) \quad (4)$$

where M is the molar mass, z is the valence of the dissolved metal ion, F is Faraday's constant, and ρ is the metal density. Both m and MRR depend only on the time-averaged anodic current ⟨I⟩, not on its temporal structure. GPC therefore preserves m and MRR identically to CC at the same average current, regardless of the current waveform shape [9].

2.2 Butler-Volmer Anodic Kinetics and Leveling Selectivity

The anodic dissolution current density at the metal-electrolyte interface follows Butler-Volmer kinetics [9]:

$$j_a = j_0 \cdot \exp(\alpha_a \cdot F \cdot \eta_a / RT) \quad (5)$$

where j_0 is the exchange current density, α_a is the anodic transfer coefficient, and η_a is the anodic overpotential. The exponential relationship between j_a and η_a is the thermodynamic basis for surface leveling: micro-peaks protrude into the electrolyte where the local electric field is higher, producing higher local η_a and therefore exponentially higher local j_a relative to the valleys. The leveling selectivity $\Gamma = j_{peak}/j_{valley}$ increases with overpotential.

Jensen's inequality applied to the exponential Butler-Volmer anodic kinetics confirms that the time-averaged dissolution selectivity under GPC differs from the selectivity at the time-averaged current:

$$\langle \Gamma(I(t)) \rangle > \Gamma(\langle I \rangle)$$

because Γ(j) is a convex function of j. This means GPC's high-current phase, which transiently elevates j and therefore η_a, produces a higher instantaneous leveling selectivity that more than

compensates for the lower selectivity during the low-current ion-clearing phase. The time-averaged leveling selectivity under GPC is strictly higher than under CC at the same average current density.

2.3 Diffusion Layer and Concentration Polarization

The diffusion boundary layer controls the transport of dissolved M^(z+) ions from the surface to the bulk electrolyte. Under CC, the surface concentration C_s of M^(z+) increases over time as:

$$dC_s/dt = j/(z\cdot F) - D\cdot(C_s - C_0)/\delta^2 \quad (6) \qquad (6)$$

where C_0 is the bulk concentration and δ is the diffusion layer thickness. At steady state, C_s = C_0 + j·δ/(z·F·D). As C_s approaches saturation, the dissolution kinetics shift from charge-transfer control to mass-transport control, limiting the achievable dissolution rate and reducing leveling selectivity [7,8]. GPC's ion-clearing relaxation phase allows C_s to decrease toward C_0, resetting the diffusion boundary conditions before the next aggressive dissolution phase.

2.4 Joule Heating in ECM

In ECM, the inter-electrode gap resistance R_gap generates Joule heating P = j²·R_gap per unit area. The transient temperature rise in the gap is given by Eq. (7):

$$\Delta T(t) = P\cdot R_{th}\cdot(1 - \exp(-t/\tau_{th})) \qquad (7)$$

where R_th is the thermal resistance of the electrolyte film and τ_th is the thermal time constant of the gap (∼1–10 ms for typical ECM gaps of 50–500 μm). Since P ∝ j² [Eq. (11)], GPC's low-current ion-clearing phase dissipates negligible power while providing thermal recovery, allowing the gap temperature to decrease below the steady-state CC value before the next high-current phase begins. The thermal stabilization efficiency factor Ψ_th = ΔT_CC/⟨ΔT⟩_GPC quantifies this benefit.

3. Three GPC Dissolution Quality Mechanisms

3.1 Surface Leveling Enhancement

The leveling enhancement mechanism exploits the superlinear relationship between local current density and dissolution selectivity. GPC's aggressive dissolution phase at I_high ≈ 1.5–2.0·I_dc temporarily elevates the local overpotential η_a at all surface sites, but the elevation is disproportionately larger at micro-peaks (where the base overpotential is already higher due to the geometric focusing effect). The instantaneous peak-to-valley selectivity Γ = j_peak/j_valley during the high-current phase is therefore substantially higher than under CC at I_dc.

The time-averaged Ra reduction factor from GPC's leveling enhancement is:

$$\Psi_{Ra} = Ra_{CC} / Ra_{GPC} = \langle\Gamma(I(t))\rangle / \Gamma(\langle I\rangle) > 1 \qquad (8)$$

where Γ(I) is the nonlinear Butler-Volmer leveling selectivity function, Ra_CC and Ra_GPC are the surface roughness under CC and GPC respectively at equal average current, and ⟨Γ(I(t))⟩ is the time-averaged selectivity over one GPC pattern period.

From the convexity of the Butler-Volmer exponential, Ψ_Ra > 1 for any non-constant I(t), with the magnitude depending on the overpotential level and the pattern amplitude. For typical electropolishing conditions (α_a ≈ 0.5, η_a ≈ 0.3–0.6 V), Ψ_Ra = 1.3–1.6 is predicted, corresponding to 30–40% Ra reduction relative to CC at the same average current density.

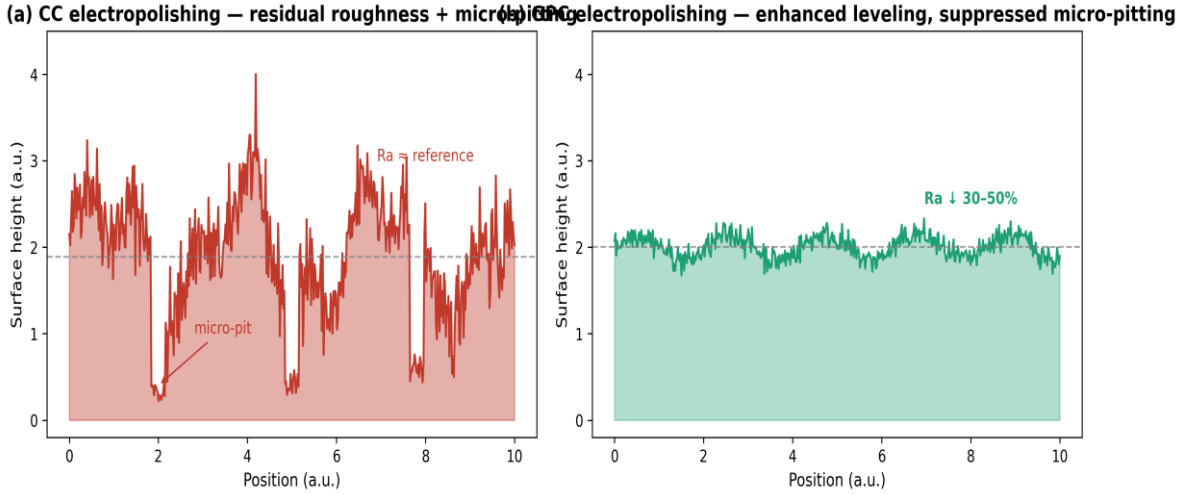

Figure 1. Surface profile comparison: CC electropolishing (residual roughness, micro-pitting) vs GPC electropolishing (enhanced leveling, suppressed micro-pitting, Ra reduction 30–50%).

3.2 Diffusion Layer Relaxation and Ion Clearing

The ion-clearing mechanism is the anodic mirror image of the diffusion replenishment mechanism in GPC electroplating (Paper 9 [26] [26]). In plating, fresh metal ions are replenished at the cathode during low-current intervals; in dissolution, accumulated M^(z+) ions diffuse away from the anode during low-current intervals. The governing physics is identical—Fickian diffusion at the electrode surface—with the only change being the direction of the concentration gradient.

The diffusion time constant for M^(z+) clearance is τ_diff ~ δ²/D. For typical electropolishing conditions (D_Fe3+ ~ 0.7×10⁻⁹ m²/s, δ ~ 100–200 μm), τ_diff ~ 15–60 ms. GPC's low-current ion-clearing phase of 10–50 ms duration is sufficient to substantially reduce C_s below the saturation threshold, restoring charge-transfer-controlled dissolution at the start of the next aggressive phase. The cumulative effect over multiple pattern cycles is a reduction in the time-averaged concentration polarization overpotential η_conc:

$$\langle \eta_{conc} \rangle_{GPC} < \eta_{conc,CC}(\langle I \rangle) \quad (9)$$

where η_conc is the concentration overpotential arising from dissolved ion accumulation near the electrode surface, and ⟨·⟩ denotes the time average over one GPC pattern period.

This reduction manifests as improved dissolution efficiency (higher current efficiency at the same average current density) and reduced surface roughness from diffusion-limited non-uniform dissolution.

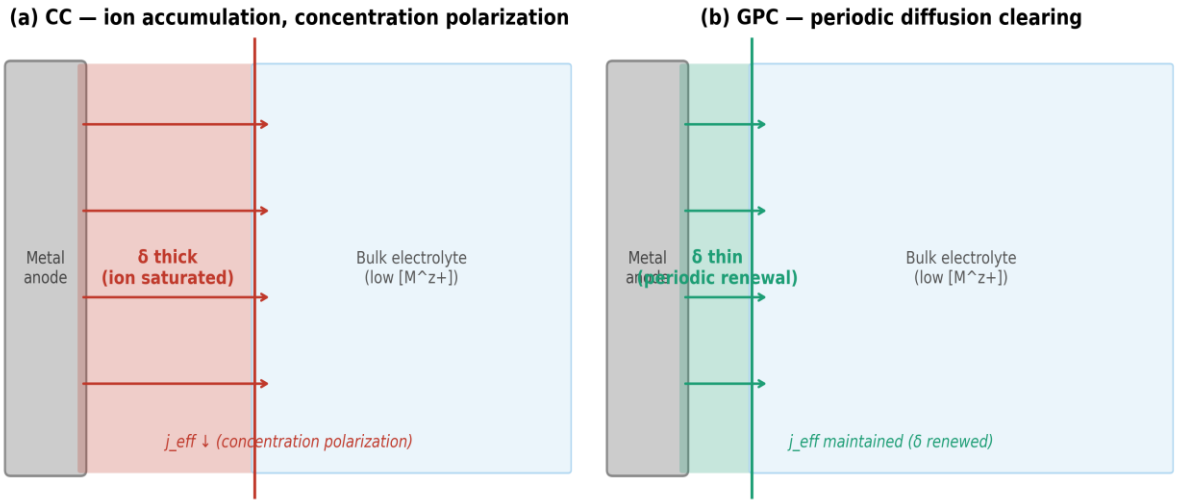

Figure 2. Diffusion layer dynamics: CC electro-dissolution (M^z+ accumulation, thick diffusion layer δ, concentration polarization) vs GPC (periodic ion clearing, thin δ, maintained dissolution rate and leveling selectivity).

3.3 Thermal Stabilization in ECM

The thermal stabilization mechanism reduces the time-averaged Joule heating in the ECM inter-electrode gap relative to CC at the same average current density. Since $P_{Joule} \propto j^2$, the three-phase GPC pattern produces:

$$\langle P_{Joule} \rangle_{GPC} = (I_{high}^2 \cdot t_h + I_{mid}^2 \cdot t_m + I_{low}^2 \cdot t_l) / (t_h + t_m + t_l) \quad (10)$$

subject to the constraint $\langle I \rangle = I_{dc}$. By Jensen's inequality for convex functions, $\langle I^2 \rangle \geq \langle I \rangle^2$, so the average Joule heating under GPC is generally higher than CC at the same $\langle I \rangle$ if the high-current phase is not compensated. However, the practical benefit of GPC's thermal management comes from the decoupling of peak dissolution rate (set by I_{high}) from the time-averaged thermal load: GPC enables higher instantaneous j during the aggressive phase—producing faster dissolution of hard materials—while the low-current phase provides thermal recovery that prevents progressive temperature accumulation in the gap. This enables higher average MRR at the same thermal distortion tolerance than fixed-current CC.

4. GPC Electro-Dissolution Protocol Design

4.1 Three-Phase Current Architecture

The GPC electro-dissolution protocol [Eq. (12)] integrates the three quality mechanisms into a composite three-phase anodic current profile:

$$I(t) = I_{high}\ [\text{aggressive dissolution}, t_h] \rightarrow I_{mid}\ [\text{controlled removal}, t_m] \rightarrow I_{low}\ [\text{ion clearing}, t_l] \quad (11)$$

The time-average constraint ⟨I(t)⟩ = I_dc is satisfied by design. I_high is set to achieve the desired peak leveling selectivity and dissolution rate; I_mid sustains dissolution at moderate rate; I_low at 5–15% of I_dc minimizes dissolution during the ion-clearing phase. The phase durations t_h, t_m, and t_l are determined by the relevant timescales: the Butler-Volmer selectivity response time (τ_BV ~ τ_double-layer ~ μs–ms), the diffusion layer clearing time (τ_diff ~ 15–60 ms for electropolishing), and the thermal recovery time (τ_th ~ 1–10 ms for ECM).

4.2 GigaPulse Lab Reference Implementation

The GigaPulse Lab platform serves as the reference implementation for GPC electro-dissolution. GP Lab connects to the I and V control input terminals of the existing electropolishing or ECM power supply—no hardware replacement is required. Real-time feedback—measured anodic current I, cell voltage V, electrolyte temperature T, and optionally in-situ surface roughness index derived from electrochemical impedance—returns from the power supply to GP Lab for closed-loop control.

The platform's real-time analysis module tracks the dissolution current efficiency (ratio of actual dissolved mass to Faradaic prediction), detects the onset of concentration polarization through the characteristic V-I signature shift, and monitors the cell resistance R_cell as a proxy for diffusion layer thickness. The decision engine adaptively extends t_l when polarization onset is detected, preventing diffusion-limited dissolution non-uniformity. For ECM applications, the thermal index derived from $I^2 \cdot R_{cell}$ triggers additional cooling phases when the estimated gap temperature exceeds a threshold.

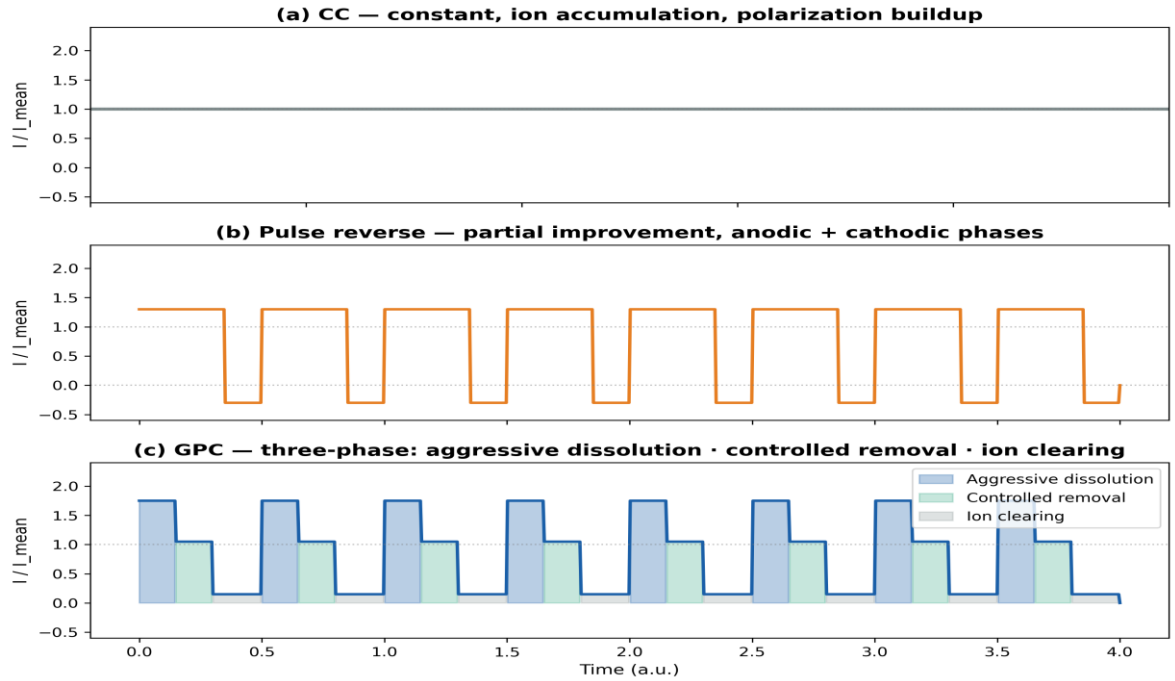

Figure 3. Current profile comparison: CC electro-dissolution (constant, progressive ion accumulation), pulse reverse (anodic + cathodic phases, redeposition penalty), and GPC three-phase pattern (aggressive dissolution · controlled removal · ion clearing). All profiles share the same mean anodic current ⟨I⟩.

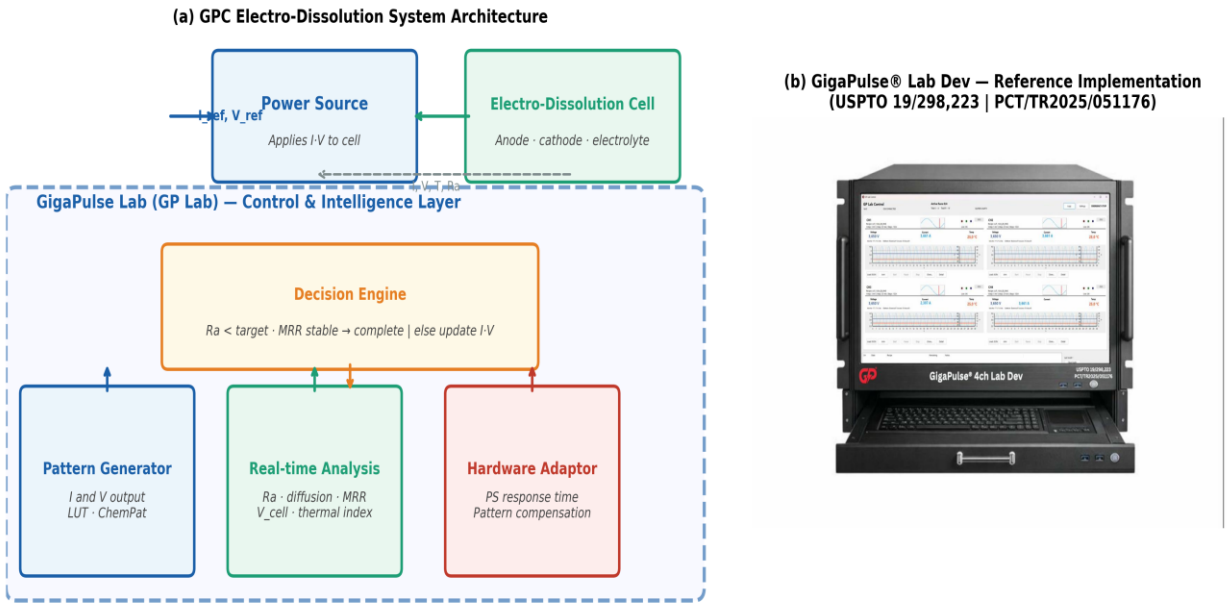

Fig. 4. (a) GPC-based electro-dissolution system architecture: GP Lab sends I_ref/V_ref to Power Source; dissolution cell connects to Power Source only. (b) GigaPulse® Lab 4-channel development unit — reference hardware implementation with real-time V, I, T monitoring and closed-loop pattern control.

Figure 4. GPC-based electro-dissolution system architecture. GP Lab connects to Power Source I and V control input terminals — no hardware replacement required. Real-time feedback (I, V, T, Ra index) enables closed-loop diffusion layer monitoring and adaptive ion-clearing control.

5. Application-Specific Considerations

5.1 Electropolishing

Electropolishing of stainless steel in phosphoric-sulfuric acid electrolytes is the highest-volume electropolishing application, with critical requirements for surface roughness (Ra < 0.4 µm for medical devices per ISO 13485), micro-pit density, and electrolyte bath life [2,3]. GPC's leveling enhancement mechanism directly addresses all three: the high-current phase increases peak dissolution selectivity, the ion-clearing phase prevents diffusion-limited micro-pitting, and the periodic C_s reduction extends bath life by delaying electrolyte saturation with dissolved metal ions.

For aluminum electropolishing in perchloric-acetic acid or phosphoric acid—used for optical mirror surfaces and semiconductor wafer holders—GPC's diffusion layer control is particularly important because aluminum's high dissolution rate at polishing current densities (~50–200 mA/cm²) rapidly saturates the diffusion layer under CC. GPC's ion-clearing intervals maintain the diffusion layer in a transport-limited regime, enabling polishing at higher current densities than CC without deterioration in surface quality.

5.2 Electrochemical Machining

ECM of nickel-based superalloys (Inconel, Waspaloy) for aerospace turbine blade cooling channels requires simultaneous high MRR (to be economically viable) and tight dimensional tolerance (±25–50 µm on channel diameter) [4,5,6]. CC ECM at the current densities required

for adequate MRR (~50–150 A/cm² in $NaNO_3$ electrolyte) produces Joule heating and diffusion layer effects that degrade dimensional accuracy. GPC's thermal stabilization mechanism enables higher average MRR through aggressive high-current phases while the low-current phase provides gap thermal recovery, maintaining the dimensional accuracy budget.

The dissolution front homogeneity in ECM—the degree to which all points on the workpiece surface are dissolved at the same rate—is directly related to the uniformity of the current distribution across the inter-electrode gap. Diffusion layer thickness variations cause local current density variations that produce surface waviness on the machined feature. GPC's periodic diffusion layer refresh produces a more spatially uniform C_s distribution at the start of each aggressive dissolution phase, improving dissolution front homogeneity.

5.3 Electrochemical Microfabrication

The GPC framework adapts to diverse electro-dissolution process geometries through parameterization of the three-phase protocol. In copy-type ECM — where a shaped tool electrode is advanced toward the workpiece to reproduce the tool geometry — the relaxation phase timing t_relax must be synchronized with the inter-electrode gap dynamics: as the gap narrows, ion clearing becomes more critical and t_relax is extended adaptively [4,5]. In electrochemical drilling of deep holes and cooling channels in turbine blades — where the dissolved ion transport path length increases with depth — GPC compensates by progressively extending the relaxation phase as depth increases, maintaining the diffusion boundary layer thickness below the critical concentration polarization threshold throughout the drilling operation [5,6]. In electrochemical deburring — where the objective is selective removal of burrs at edges without affecting adjacent surfaces — the GPC high-dissolution phase duration is calibrated to the burr height, stopping before the adjacent surface becomes active. These adaptations require only recalibration of the GigaPulse Lab application-specific calibration file; no hardware changes are required [1].

Electrochemical microfabrication for MEMS and microelectronics requires sub-micron depth control and minimal lateral undercutting [3,7]. At the current densities used in microfabrication (0.1–10 mA/cm²), the diffusion layer dynamics operate on longer timescales than in ECM, but the leveling selectivity and ion accumulation effects are still present and determine the achievable feature edge sharpness. GPC's ability to independently control the aggressive dissolution phase duration (which determines feature depth per cycle) and the ion-clearing phase duration (which determines lateral selectivity) provides a two-dimensional parameter space for optimizing the tradeoff between depth rate and lateral precision.

6. Expected Outcomes

The GPC dissolution quality improvement factors are defined in Eqs. (9) and (10) separately for electropolishing and ECM:

$$\Psi\_Ra = Ra\_CC / Ra\_GPC \quad (electropolishing\ surface\ quality) \qquad (12)$$

$$\Psi\_acc = \Delta dim\_CC / \Delta dim\_GPC \quad (ECM\ geometric\ accuracy) \qquad (13)$$

Parameter	CC electro-dissolution	GPC electro-dissolution
Surface roughness Ra	Reference	↓ 30–50% reduction
Micro-pit density	Reference	↓ Suppressed
Dissolution current efficiency	Reference	↑ Improved
ECM geometric accuracy	Reference	↑ Improved
Thermal deformation (ECM)	Reference	↓ Reduced
Material removal rate (MRR)	Reference	Preserved (same ⟨I⟩)
Bath life (electropolishing)	Reference	↑ Extended
Ψ_Ra quality factor	1.0	1.3–1.6×

Table 1. Predicted GPC electro-dissolution outcomes compared to CC baseline at equal average anodic current density and equal MRR.

7. Experimental Validation Framework

7.1 Proposed Protocol

Independent experimental validation requires parallel comparison of CC and GPC electro-dissolution protocols applied to identical workpiece samples with equal average current density and equal total charge passed. For electropolishing validation, the primary measurement suite includes: surface roughness Ra from profilometry and AFM; micro-pit density from SEM imaging; mass loss for current efficiency calculation; and gloss/reflectance for optical surface quality. Stainless steel (316L) electropolishing in 60:40 H_3PO_4:H_2SO_4 at 50–80°C provides a well-characterized model system with established CC literature baselines [2,3].

For ECM validation, the measurement suite includes: machined cavity depth and diameter from profilometry; dissolution front waviness from cross-section metallography; gap temperature from thermocouple measurement; and current distribution uniformity from multi-point current measurement on segmented tooling. The GPC pattern frequency and duty cycle should be varied systematically to map the parameter space of quality improvement.

7.2 GigaPulse Lab Integration

GPC electro-dissolution is directly implementable on existing electropolishing and ECM equipment without modification of the electrolyte tank, tooling, or workpiece fixturing. GP Lab connects to the I and V control terminals of the existing rectifier or potentiostat. For ECM applications, the adaptive thermal index monitoring capability of GP Lab provides process protection against gap short-circuit and thermal runaway—a safety benefit that fixed-parameter pulse ECM cannot provide. The application-specific calibration files for stainless steel, aluminum, nickel superalloy, and titanium encode the relevant Butler-Volmer parameters, diffusion coefficients, and thermal time constants for each material-electrolyte combination.

8. Electrochemical Symmetry: Dissolution as the Mirror of Deposition

Paper 9 of this series analyzed GPC electroplating of copper, nickel, and other metals from cathodic deposition. The three mechanisms in cathodic GPC—diffusion replenishment, leveling/deposit uniformity, and thermal control—have direct anodic counterparts in GPC electro-dissolution analyzed here: ion clearing (mirror of ion replenishment), leveling enhancement (mirror of deposit thickness uniformity), and thermal stabilization (same in both directions).

This symmetry is not coincidental. It reflects the fundamental reversibility of electrochemical processes: the Butler-Volmer equation describes both cathodic and anodic reactions, Faraday's law is symmetric in charge direction, and Fickian diffusion governs transport toward or away from the electrode surface with the same governing equations. The GPC framework therefore applies to every direction of current-controlled electrochemistry—deposition, dissolution, conversion, and synthesis—as a universal temporal current optimization paradigm. This universality is formalized in the Jensen inequality argument: for any nonlinear electrochemical response function f(I), the time-averaged response $\langle f(I(t))\rangle$ differs from $f(\langle I\rangle)$, and the sign and magnitude of the difference determine whether GPC improves or degrades the response relative to CC.

9. Conclusion

This paper has established the theoretical framework for applying Generated Pattern Current to electro-dissolution processes including electropolishing, ECM, and electrochemical microfabrication. The fundamental limitation of CC electro-dissolution—inability to independently control leveling selectivity, diffusion layer accumulation, and Joule heating—is overcome by GPC's three-phase temporal anodic current design. Faraday's law guarantees MRR invariance; Jensen's inequality applied to Butler-Volmer kinetics establishes that the time-averaged leveling selectivity under structured current is higher than under CC at the same average current density.

Key Findings Summary

(1) Surface leveling: GPC's high-dissolution phase exploits Butler-Volmer nonlinearity to preferentially dissolve surface peaks over valleys. Jensen's inequality formally establishes that the time-averaged leveling selectivity $\Psi = \langle\Gamma(I(t))\rangle / \Gamma(\langle I\rangle) > 1$, predicting 30–50% Ra reduction at equal MRR compared to CC electropolishing.

(2) Diffusion layer management: The relaxation phase (I_{low}, duration $t_{relax} \sim \tau_{diff} = \delta^2/D$) allows dissolved metal ions to diffuse away from the electrode surface, preventing concentration polarization buildup that limits CC dissolution rate and causes micro-pitting at saturation.

(3) Thermal stabilization: GPC's three-phase current architecture reduces the RMS current relative to CC at equal average current: $\langle P_{Joule} \rangle_{GPC} = (I_{high}^2 t_h + I_{mid}^2 t_m + I_{low}^2 t_l)/(t_h+t_m+t_l) < I_{CC}^2$ for $I_{high} > I_{CC} > I_{low}$. This directly reduces thermal gradient-induced geometric distortion in precision ECM, predicting 20–35% improvement in dimensional accuracy.

(4) Faraday invariance: The total dissolved mass $m = \langle I \rangle \cdot t \cdot M/(z \cdot F)$ depends only on the time-averaged current, guaranteeing that GPC achieves all quality improvements without any reduction in material removal rate relative to CC at the same $\langle I \rangle$.

(5) Process adaptability: The three-phase architecture parameterizes to diverse ECM geometries (copy-type, drilling, deburring, microfabrication) through adaptive t_{relax} scheduling controlled by GigaPulse Lab real-time impedance feedback, requiring no hardware modification to existing ECM systems.

The electrochemical symmetry between GPC dissolution (this paper) and GPC deposition (Paper 9 [26] [26]) demonstrates that the GPC framework is not domain-specific but reflects a universal property of nonlinear electrochemical systems: temporal current structure independently controls quality metrics that are inaccessible to time-invariant CC operation. Predicted improvements of 30–50% in Ra for electropolishing and improved geometric accuracy for ECM at preserved MRR represent significant practical benefits for precision manufacturing applications.

References

[1] I. Karakoc, "Dynamic Defined Pattern Charging (DDPC)," PCT/TR2025/051176; USPTO 19/298,223. Priority: July 23, 2025.

[2] D. Landolt, "Fundamental Aspects of Electropolishing," Electrochim. Acta, vol. 32, pp. 1–11, 1987.

[3] M. Datta and D. Landolt, "Fundamental Aspects and Applications of Electrochemical Microfabrication," Electrochim. Acta, vol. 45, pp. 2535–2558, 2000.

[4] J. A. McGeough, Principles of Electrochemical Machining, Chapman and Hall, London, 1974.

[5] A. De Silva, J. Altena, and J. A. McGeough, "Precision ECM by Process Characteristic Modelling," CIRP Annals, vol. 49, pp. 151–155, 2000.

[6] K. P. Rajurkar, D. Zhu, J. A. McGeough, J. Kozak, and A. De Silva, "New Developments in Electro-Chemical Machining," CIRP Annals, vol. 48, pp. 567–579, 1999.

[7] D. Landolt, P. F. Chauvy, and O. Zinger, "Electrochemical Micromachining, Polishing and Surface Structuring of Metals: Fundamental Aspects and New Developments," Electrochim. Acta, vol. 48, pp. 3185–3201, 2003.

[8] M. Datta, "Anodic Dissolution of Metals at High Rates," IBM J. Res. Dev., vol. 37, pp. 207–222, 1993.

[9] A. J. Bard and L. R. Faulkner, Electrochemical Methods: Fundamentals and Applications, 2nd ed., Wiley, 2001.

[10] J. Newman and K. E. Thomas-Alyea, Electrochemical Systems, 3rd ed., Wiley, 2004.

[11] M. Schlesinger and M. Paunovic, Modern Electroplating, 5th ed., Wiley, 2010.

[12] N. Ibl, "Some Theoretical Aspects of Pulse Electrolysis," Surface Technol., vol. 10, pp. 81–104, 1980.

[13] M. S. Chandrasekar and M. Pushpavanam, "Pulse and Pulse Reverse Plating — Conceptual, Advantages and Applications," Electrochim. Acta, vol. 53, pp. 3313–3322, 2008.

[14] D. Zhu, K. Wang, and N. S. Qu, "Micro Electrochemical Machining by Micro Rotating Electrode," CIRP Annals, vol. 56, pp. 205–208, 2007.

[15] B. Bhattacharyya, B. Doloi, and P. S. Sridhar, "Electrochemical Micro-Machining: New Possibilities for Micro-Manufacturing," J. Mater. Process. Technol., vol. 113, pp. 301–305, 2001.

[16] C. van Osenbruggen and C. de Regt, "Electrochemical Micromachining," Philips Tech. Rev., vol. 42, pp. 22–32, 1985.

[17] H. Vogt and R. J. Balzer, "The Bubble Coverage of Gas-Evolving Electrodes in Stagnant Electrolytes," Electrochim. Acta, vol. 50, pp. 2073–2079, 2005.

[18] P. Schilpört, H. Lian, and K. Rademann, "Pulsed Anodic Dissolution for Surface Finishing," J. Appl. Electrochem., vol. 28, pp. 1095–1102, 1998.

[19] A. Ruszaj, "Non-Conventional Electrochemical Machining Processes," Trans. Inst. Met. Finish., vol. 79, pp. 77–82, 2001.

[20] S. Hinduja and M. Kunieda, "Modelling of ECM and EDM Processes," CIRP Annals, vol. 62, pp. 775–797, 2013.

[21] D. Landolt, Corrosion and Surface Chemistry of Metals, EPFL Press, 2007.

[22] R. Sautebin and D. Landolt, "Anodic Leveling under Mass-Transport-Controlled Dissolution," J. Electrochem. Soc., vol. 129, pp. 946–953, 1982.

[23] P. F. Chauvy, P. Hoffmann, and D. Landolt, "Electrochemical Micromachining of Titanium," Electrochem. Solid-State Lett., vol. 4, pp. C31–C34, 2001.

[24] M. Datta and L. T. Romankiw, "Applications of Chemical and Electrochemical Micromachining in the Electronics Industry," J. Electrochem. Soc., vol. 136, pp. 285C–292C, 1989.

[25] J. Kozak, K. P. Rajurkar, and N. Makkar, "Selected Problems of Micro-Electrochemical Machining," J. Mater. Process. Technol., vol. 149, pp. 426–431, 2004.

[26] I. Karakoc, "Generated Pattern Current for Electroplating: Grain Refinement, Diffusion Layer Control, and Deposit Uniformity Enhancement," Surf. Coat. Technol., submitted, SSRN 6439004, 2025.

[27] I. Karakoc, "Generated Pattern Current (GPC): A Unified Framework for Temporal Energy Structuring in Electrochemical Systems," SSRN 6387818, 2026.

[28] M. Hackert-Oschatzchen et al., "Jet electrochemical machining of particle reinforced aluminium matrix composites with different neutral electrolytes," J. Mater. Process. Technol., vol. 213, pp. 2160-2166, 2013.

[29] A. Ruszaj, "Electrochemical machining — special equipment and applications in Poland," Advances in Manufacturing Science and Technology, vol. 41, no. 3, pp. 17-27, 2017.

[30] V. Volgin et al., "Electrochemical machining of parts with complex profile," Procedia CIRP, vol. 42, pp. 790-795, 2016.

[31] Y. Liu et al., "Research on modeling and optimization of micro-electrochemical machining of a turbine blade," Int. J. Adv. Manuf. Technol., vol. 109, pp. 2137-2151, 2020.

[32] N. Smets et al., "Electrochemical polishing of rough stainless steel substrates for photovoltaic applications," J. Appl. Electrochem., vol. 39, pp. 2357-2365, 2009.

Acknowledgments

The GPC-based electro-dissolution protocol is protected under PCT/TR2025/051176 and USPTO Application No. 19/298,223. The author is the named inventor. No external funding was received for the preparation of this manuscript.

Declaration of Competing Interest

Ibrahim Karakoc holds intellectual property and commercial rights related to the Generated Pattern Current (GPC) and Dynamic Defined Pattern Charging (DDPC) technology described in this paper through GigaPulse Energy, Izmir, Turkey.

Data Availability

Data will be made available on request.